National Aeronautics and Space Administration

Orbital Debris
Quarterly News

Volume 28, Issue 3
July 2024

A publication of the
NASA Orbital Debris
Program Office (ODPO)

NASA Issues Its First Space Sustainability Strategy

NASA Deputy Administrator Pam Melroy announced the release of Volume 1: Earth Orbit, of NASA's Space Sustainability Strategy during the Space Symposium on 9 April 2024. NASA's Space Sustainability Strategy aims to cover four domains: on Earth, in Earth orbit, in cislunar space (including the Lagrange points and the lunar surface), and in deep space. The purpose of the strategy is to focus on advancements the Agency can make that address the mounting space sustainability challenges posed by the rapidly changing space environment and that are aligned with NASA's mission as a science and technology organization.

Volume 1 of the strategy focuses on sustainability in Earth orbit and has identified five major challenges: 1) A single framework for space sustainability has not been accepted by the space community. 2) Current metrics and modeling are not sufficient to support holistic frameworks. 3) Uncertainties in the space environment and space operations are a main driver of risks to space sustainability. 4) Space sustainability may be in tension with other mission interests. 5) Space sustainability is a global issue that requires a coordinated, multilateral response.

To address these challenges, NASA commits to pursue the following goals for space sustainability in Earth's orbit. Each goal is followed by objectives that will guide NASA's achievement of the goals.

Goal 1	Develop a framework for assessing space sustainability at NASA.
Goal 2	Prioritize the most efficient ways to minimize uncertainties about orbital debris and operations in the space environment.
Goal 3	Lower barriers to space sustainability through developing and transferring technology.
Goal 4	Update or develop policies that provide incentives to support space sustainability.
Goal 5	Continue and improve coordination and collaboration outside of NASA.
Goal 6	Improve NASA's internal organization to support space sustainability.

NASA's new strategy for space sustainability begins in Earth Orbit

Space Sustainabilty
continued from page 1

"The release of this strategy marks true progress for NASA on space sustainability," said NASA Deputy Administrator Pam Melroy. "Space is busy – and only getting busier. If we want to make sure that critical parts of space are preserved so that our children and grandchildren can continue to use them for the benefit of humanity, the time to act is now. NASA is making sure that we're aligning our resources to support sustainable activity for us and for all." [1]

NASA's Space Sustainability Strategy Volume 1: Earth Orbit is publicly available at: https://www.nasa.gov/wp-content/uploads/2024/04/nasa-space-sustainability-strategy-march-20-2024-tagged3.pdf.

References
1. NASA Press Release, 09 April 2024, https://www.nasa.gov/news-release/new-nasa-strategy-envisions-sustainable-future-for-space-operations/. ♦

Updates to the NASA Procedural Requirements for Orbital Debris Mitigation

The NASA Procedural Requirements for Orbital Debris Mitigation, NPR 8715.6, was updated to revision E and became official on 19 April 2024. This high-level NASA policy document defines responsibilities and procedural requirements for the planning, implementation, and review of orbital debris mitigation measures for NASA-sponsored spaceflight activities, consistent with the U.S. National Space Policy, the U.S. Government Orbital Debris Mitigation Standard Practices, and NASA's policy to protect the orbital space environment.

Revision E focuses on orbital debris mitigation in Earth orbit but recognizes the relevance of orbital debris mitigation in cislunar and other environments. It also provides clarifications for missions subject to commercial regulations; removes the operational conjunction assessment aspect from the document; streamlines the Orbital Debris Assessment Report (ODAR) and End of Mission Plan (EOMP) submission and review process; and establishes notification protocol for NASA object reentries and risk assessments associated with new on-orbit fragmentation events.

NPR 8715.6E reestablishes the roles and responsibilities of the NASA Orbital Debris Program Office as the following:

a. Collects measurement data to characterize the orbital debris populations and the ever-changing orbital debris environment.

b. Maintains and leads the advancement of orbital debris models, assessment tools and mitigation standards.

c. Provides technical evaluations of the ODARs and EOMPs.

d. Tracks the compliance with orbital debris mitigation measures by NASA programs and projects.

e. Assists USG departments and agencies on matters related to the characterization of the orbital debris environment and the application of orbital debris mitigation measures and policies.

f. Contributes to the determination, adoption, and use of international orbital debris mitigation guidelines through international fora such as the United Nations Committee on the Peaceful Uses of Outer Space, the IADC, and ISO.

NPR 8715.6E is available at: https://nodis3.gsfc.nasa.gov/npg_img/N_PR_8715_006E_/N_PR_8715_006E_.pdf. ♦

Subscribe to the ODQN or Update Your Subscription Information

To be notified by email when a new issue of the ODQN is placed online, or to update your personal information, please navigate to the ODQN subscription page on the NASA Orbital Debris Program Office (ODPO) website at: https://orbitaldebris.jsc.nasa.gov/quarterly-news/subscription.cfm. The ODPO respects your privacy. Your email address will be used solely for communication from the ODQN Managing Editor.

PROJECT REVIEW
Laboratory Radar Cross Section Measurements

J. ARNOLD HEADSTREAM AND A. MANIS

A fundamental characteristic required to model the orbital debris environment is the size of orbital debris objects, especially fragmentation debris. This quantity is not directly measured by radars but must be inferred from the measured radar cross section (RCS). To interpret the observed RCS of orbital debris objects detected by radars as physical sizes, NASA uses an empirical size estimation model (SEM) developed in 1990 and 1991 based on laboratory measurements of breakup fragments generated in hypervelocity impact tests as well as fragments fabricated by NASA and subsequently measured in a radar range [1, 2]. While the fragments measured from those ground-based tests were considered representative of a generic spacecraft collision at the time, the materials, construction techniques, and technology used to build spacecraft has evolved and more modern, lightweight materials are now more prevalent. A ground-based hypervelocity impact experiment was conducted in 2014 that incorporated a high-fidelity engineering model representative of a low Earth orbit spacecraft, referred to as DebriSat [3]. One of the primary goals of DebriSat was to collect fragments down to 2 mm in size and to characterize them in terms of size, mass, area-to-mass ratio, density, shape, and material composition to inform updates to

Table. List of 16 Calibration Targets Measured with Shape, Material Type and Dimensions. SS=stainless steel, Al=Aluminum, CFRP= Carbon Fiber Reinforced Polymer, PCB = printed circuit board Cu=Copper

| Test	Shape	Material	Dimensions		
			Diameter	Length	Thickness
1	Sphere	SS, polished	2.4 cm	--	--
2	Sphere	SS, polished	1 cm	--	--
3	Sphere	SS, polished	6 mm	--	--
4	Sphere	SS, polished	3 mm	--	--
5	Rod	SS, polished	3.175 mm	3 cm	--
6	Rod	SS, ground	1.588 mm	1 cm	--
7	Square Plate	Al, polished	--	3 cm x 3 cm	3.175 mm
8	Round Plate	CFRP, twill	7.62 cm	--	2.921 mm
9	Square Plate	CFRP, twill	--	15.24 cm x 15.24 cm	2.921 mm
10	Rod	CFRP	3.175 mm	3 cm	--
11	Square Plate	FR4 (PCB)	--	3 cm x 3 cm	1.57 mm
12	Square Plate	CFRP, unidirectional	--	30.48 cm x 30.48 cm	2.54 mm
13	Square Plate	CFRP, quasi-unidirectional	--	30.48 cm x 30.48 cm	1.397 mm
14	Round Plate	Al	3 cm	--	3.175 mm
15	Rod	CFRP, unidirectional	3.175 mm	4 cm	--
16	Rod	Cu	3.175 mm	4 cm	--
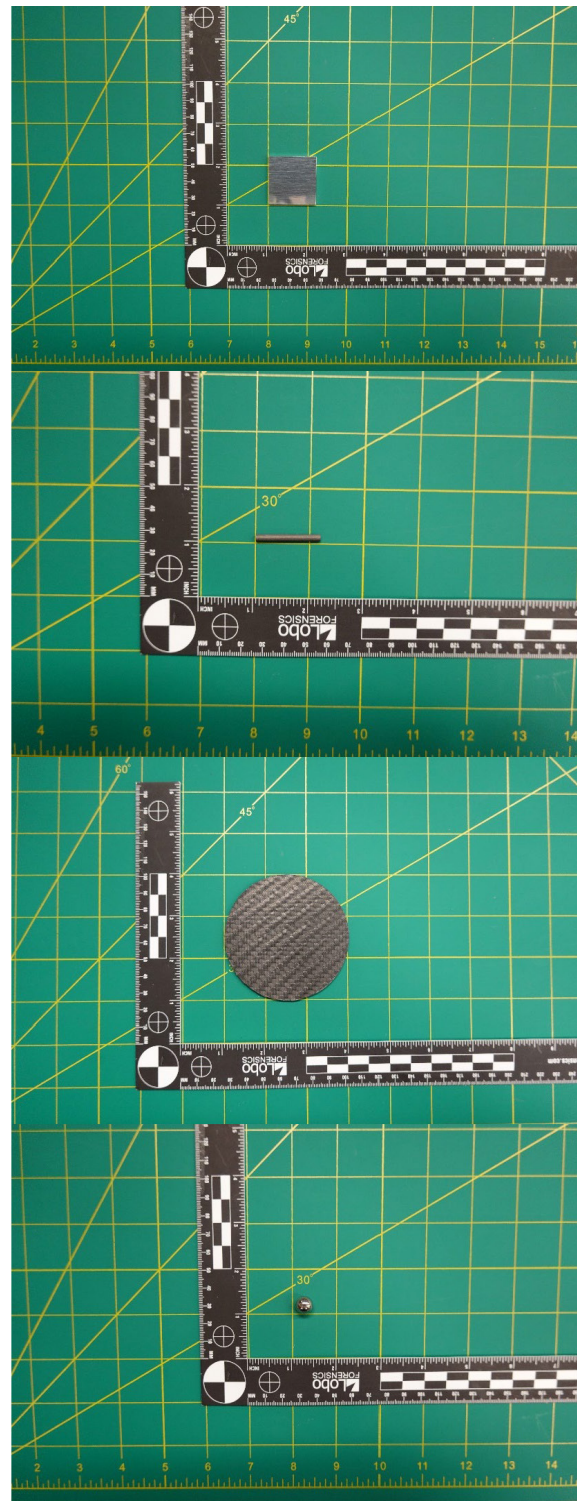
Figure 1. A selection of the radar calibration targets (top to bottom): a polished aluminum square plate; a CFRP rod; a flat, round CFRP twill plate; and a stainless-steel sphere.

3

Radar Measurements

NASA's Standard Satellite Breakup Model (SSBM) (ODQN vol. 18, issue 3, pp. 3-5).

A subset of the DebriSat fragments will be selected to update each of the NASA SEM's, radar and optical, using a new suite of laboratory measurements. Because many of the DebriSat fragments have complex shapes and/or are composed of multiple materials, it is necessary to evaluate the capabilities and limitations of the laboratory measurements before selecting fragments for further analysis. A set of calibration targets with well-defined geometries and material compositions were chosen for such an evaluation. Calibration target shapes include spheres, flat plates, and cylinders. As with DebriSat, calibration target materials were chosen to represent typical modern-day spacecraft components and include stainless steel, aluminum, printed circuit board (PCB) substrate, and carbon fiber-reinforced polymer (CFRP). These materials also represent a wide range of

Figure 2. View of the OSU-ESL compact radar range showing the reflector on the back wall and the rotating low density foam positioner in the center. The chamber is lined with RF absorptive wedges designed to minimize reflection of RF waves from the walls.

electrical conductivities, which strongly influences measured RCS and inferred target size. A total of 16 calibration targets were measured, with characteristics listed in the Table and examples shown in Figure 1. The CFRP targets have various weaves and surface textures including: twill, with a reflective gloss surface on one side and a matte texture on the reverse; unidirectional, with a gloss surface on both sides and fibers running in a single direction; and quasi-unidirectional, with a woven texture where bundles of CFRP fibers are held together with plastic "string."

Calibration measurements were conducted in The Ohio State University's ElectroScience Laboratory (OSU-ESL) compact radar range. The facility's foam test positioner, shown in Figure 2, is mounted on a large, motorized rotator and can rotate a full 360° in azimuth. The ESL can measure from 2 to 18 GHz with a single setup and can cover 1 to 2 GHz with a second setup. The radar range calibration targets were measured with the 2 to 18 GHz configuration. A frequency sweep is conducted at each azimuth angle over a range of predefined azimuth angles as the foam positioner is rotated. A full set of RCS measurements in frequency and azimuth takes roughly 10 to 15 minutes to complete depending on the number of angles and angular step size used. Each transmit (first letter)-receive (second letter) combination of horizontal (H) and vertical (V) linear polarization, denoted HH, VV, VH, or HV, can be collected in separate measurements, for a total of roughly 40 to 60 minutes per calibration target. RCS measurements were collected over a full 360° in azimuth in 5° azimuth increments for the spheres and in 1° azimuth increments for all other calibration targets. Due to the symmetry of the calibration targets, the measurements in azimuth were conducted at a single elevation of 0°. As shown in Figure 3, the samples were placed in custom-made sample holders fabricated from low dielectric constant, low-loss structural foam that rested on the large rotating positioner.

The left panel of Figure 4 shows a polar plot of the azimuthally dependent RCS of 2 different rods (Test object #15 and #16) as measured in the OSU-ESL radar range at a frequency of 10 GHz. These rods have the same dimensions but are made of two different materials with quite different dielectric constants: CFRP and copper. Copper is extremely conductive, ~5 x 10^7 siemens per meter (s/m). In contrast, CFRP is only somewhat conductive. Its conductivity depends a lot on the exact composite used, but it is roughly 3 to 4 orders of magnitude lower than copper. The length of the rod is perpendicular to the transmitted beam at 0° and 180°, and the circular cross section of the ends of each rod are perpendicular to the transmitted beam at 90° and 270°. Despite the difference in electrical conductivity between these two materials, both targets
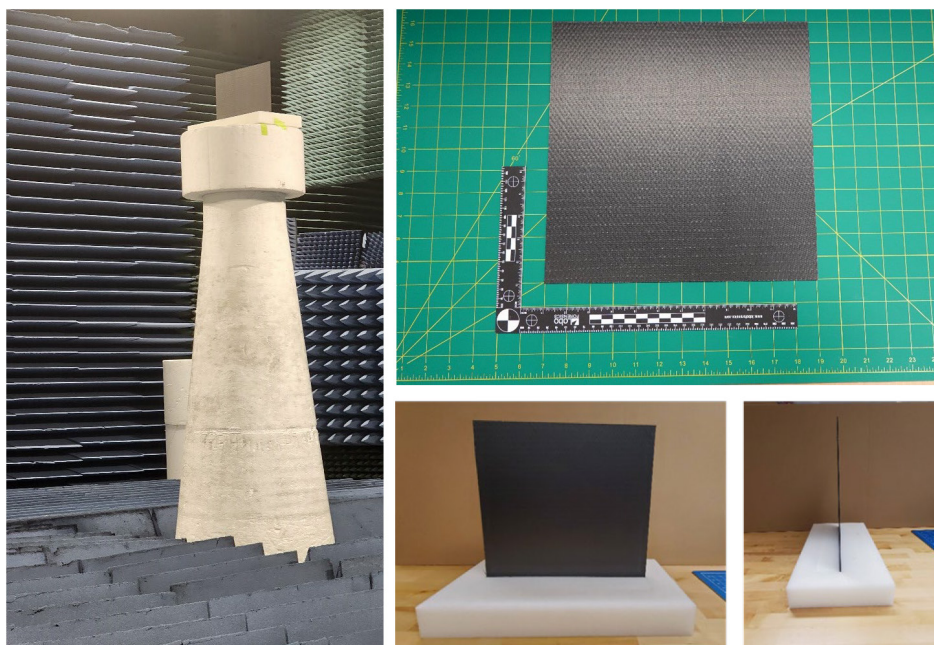

Figure 3. Left: target and holder placed on rotating foam positioner pedestal in the OSU-ESL radar range. Top right: example of one of the calibration targets, a CFRP square plate. Bottom right: two views of the same target in a custom-made low loss foam sample holder.
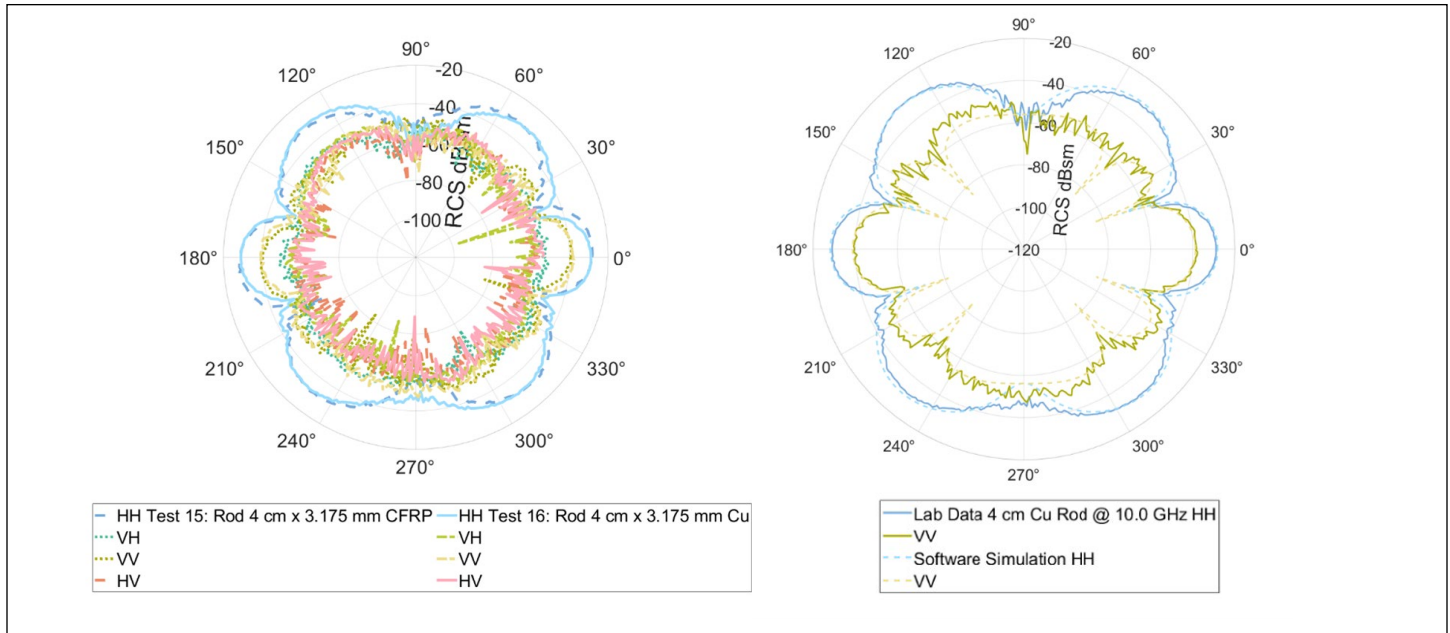
Radar Measurements

Figure 4. Left: Laboratory measured RCS over a 360° sweep in azimuth angle at a frequency of 10 GHz for two targets of similar dimensions but different compositions; CFRP rod and copper rod, respectively. Right: Comparison between RCS measurements and software simulation results for the 4 cm copper rod. The HH polarization configuration compares well between the lab measurements and the RCS simulation. The VV component compares well near 0° and 180° incidence and is beneath the noise floor of the lab RCS measurements at other incidence angles.

show a similar azimuthally dependent RCS. The HH principal polarization measurements, where the reflected signal has the same horizontal polarization as the transmitted electromagnetic (EM) wave, have good signal to noise ratio and are similar between the two materials. The returns are strongest when the long edge of the rod faces perpendicular or at a 45° angle to the transmitted EM wave, and close to the noise floor when the small reflecting area of the ends of the rod face the transmitted wave. The VV principal polarization measurements have good signal to noise ratio near 0° and 180°, where the most surface area is perpendicular to the transmitted beam. The difference between the HH and VV signals is due to the linear shape of the rod. The cross-polar measurements HV and VH are below the ~-50 dBsm noise floor of the measurements.

Due to the large number of fragments that were generated from the DebriSat test (~300,000), only a subset of statistically representative fragments will be used in future RCS measurements to inform SEM analyses. Fragment selection will need to account for laboratory instrumental limitations such as the minimum detectable size of various materials. To support the evaluation of RCS laboratory measurement capabilities and limitations the NASA Orbital Debris Program Office is evaluating the feasibility of using computational electromagnetic (CEM) modeling software to verify the initial laboratory calibration dataset. Such software can compute the RCS of high-conductivity targets with non-spherical shapes. The right panel of Figure 4 shows a comparison between the measured RCS and software simulated RCS for one of the calibration targets, a copper rod (Test object #16), where

the transmitted EM beam is perpendicular to the length of the rod at 0°. The figure demonstrates good agreement between the laboratory measurements and model for the HH polarization configuration, while the simulated VV signal agrees well between the two models, but is below the noise floor of the lab measurements at angles far from 0° and 180°. This is because the cross-sectional area of the length of the rod is much larger than that of each end.

The next step toward an updated radar SEM is to develop sample holders with elevation mounts so that the complex shapes of the DebriSat fragments can be measured in both azimuth and elevation. Subsequent radar range RCS measurements will focus on evaluating possible sample holder materials with higher durability than the low-loss foam used for the calibration measurements and measuring additional calibration targets with more complex shapes such as bent plates or rods in preparation for the more complex DebriSat fragment shapes.

References

1. Xu, Y.-L. and Stokely, C. "A Statistical Size Estimation Model for Haystack and HAX Radar Detections," 56th International Astronautical Congress, Fukuoka, Japan, (2005).

2. NASA ODPO, "Handbook for Limiting Orbital Debris," NASA-Handbook 8719.14 (2008).

3. Cowardin, H., *et al*. "Updates on the DebriSat Hypervelocity Experiment and Characterization of Fragments in Support of Environmental Models," International Journal of Impact Engineering, volume 180, October 2023, 104669. ♦

Experimental Hypervelocity Impacts of Non-spherical Projectiles on Whipple Shields

J. MILLER, E. CHRISTIANSEN, C. CLINE, AND H. COWARDIN

The DebriSat hypervelocity impact (HVI) experiment performed at the Arnold Engineering Development Center in April 2014 was conducted to update the catastrophic break-up models for modern spacecraft [1, 2]. To this end, DebriSat was built with modern materials, including structural panels of carbon-fiber reinforced polymer (CFRP), multilayered insulation, solar panels, as well as typical spacecraft components. Fragments from the DebriSat impact test were captured by and extracted from porous catcher panels for characterization [3]. To date, a key observation is that CFRP fragments represent a large fraction of the collected debris and that these fragments tend to be thin, flake-like structures or long, needle-like structures; whereas debris with nearly equal dimensions is less prevalent [4]. Additionally, high-density metals like steel and copper are also prevalent and of special concern, considering orbital debris (OD) particles made of these higher density materials are more difficult to protect against. As current ballistic-limit equations (BLE) for common spacecraft shields are based on impact testing using spherical impactors, the DebriSat experiment has emphasized the need to develop broad-ranging, non-spherical, BLE [5]. The following article will highlight how the results from the DebriSat experiment have provided a path forward for evaluating non-spherical projectiles and the associated risk.

The NASA Hypervelocity Impact Technology (HVIT) group at the Johnson Space Center has developed and evaluated spacecraft micrometeoroid and orbital debris (MMOD) shielding for spacecraft (crewed and non-crewed) and designed operational techniques to reduce MMOD risk for over 30 years [6]. The team assesses MMOD risk to NASA missions using the Bumper code and the latest versions of the NASA Orbital Debris Program Office's (ODPO) Orbital Debris Engineering Model (ORDEM) and the NASA Meteoroid Environment Office's Meteoroid Engineering Model. Bumper code evaluates risk for spacecraft based on a BLE for each shield that is developed from laboratory impact experiments and hydrocode simulations.

During the review process for ORDEM 3.0 and Bumper, the National Research Council (NRC) and NASA Engineering and Safety Center (NESC) both recommended the inclusion of non-spherical projectiles into future versions of these models and tools. Specifically, the NRC recommendation stated that the ODPO's next version of ORDEM should be released as often as feasible to account for major changes to the environment or improved characterization of the OD environment, including characterization of debris shape, as applicable. In addition, the NESC recommended that the ODPO and HVIT should use laboratory HVI test data and other possible data sources to categorize debris shapes and define the relationship between characteristic length and mass/shape, incorporating this relationship into ORDEM and Bumper to determine MMOD risk. NASA's HVIT group conducted preliminary studies of graphite-epoxy projectile shape on ballistic limits of high-risk areas on the International Space Station (ISS) in U.S. Government Fiscal Year 2018. Starting from the following year, NASA's Office of Safety

and Mission Assurance has continued to provide funding for HVIT assessments of non-spherical debris that would directly benefit the development of the next ORDEM release.

The HVIT group, in coordination with the ODPO and the Remote Hypervelocity Test Laboratory (RHTL) at the NASA White Sands Test Facility in Las Cruces, New Mexico, have developed

Table. Shape Effect Experiments of Shield Types Performed to Anchor Numerical Simulations as of 30 April 2024

Shield Type	Shield Category	Number of Shots	Projectile Types	L:D
Aluminum Whipple shield with MLI thermal blanket (Key ISS risk driver)	Double Wall Shield	26	CFRP Steel Copper	1:5 1:3 2:3 3:1
Aluminum Whipple shield (common structural shield)	Double Wall Shield	9	CFRP Steel Copper	1:3 2:3 3:1
MLI Whipple shield (common ultra-light weight shield)	Double Wall Shield	8	CFRP Steel Copper	1:3 3:1
Aluminum plate (common structural material)	Monolithic Shield	4	CFRP Steel Copper	1:3 3:1
Ti6Al4V plate (common structural material)	Monolithic Shield	5	CFRP Steel Copper	1:3 2:3 3:1
Steel plate (common structural material)	Monolithic Shield	2	Steel Copper	1:3 3:1
Copper plate (common electrical conductor)	Monolithic Shield	2	Steel Copper	1:3 3:1
Alumina-enhanced-thermal-barrier (thermal protection material)	Porous Monolithic Shield	10	CFRP Steel Copper	1:3 2:3 3:1
SpaceX-proprietary-ablator-material (thermal protection material)	Porous Monolithic Shield	5	CFRP Steel Copper	1:3 2:3 3:1
MMOD enhanced thermal blanket (adaptive blanket for spot protection of critical structure)	Multi-shock Shield	4	Steel Copper	1:3 3:1
Stuffed-Whipple shield (common variant of Whipple shield with Nextel and Kevlar blankets added at the mid-point of the shield)	Multi-shock Shield	8	CFRP Aluminum Steel Copper	1:4 1:3 3:1 4:1

Whipple Shields

techniques to reliably accelerate non-spherical projectiles to approximately 7 km/s and analyze the precise orientation of the projectile at impact. These impact tests launch right-circular cylinder (RCC) projectiles of various length-to-diameter (L:D) ratios using RHTL two-stage light-gas guns (LGGs).

These projectiles are separated from the sabot as they enter the target tank, where they proceed to the target. Specialized high-speed cameras are used to image the projectile during flight and determine its state and orientation at impact, and to image the impact ejecta and debris cloud (impact debris that passes through the coupon/shield wall) for multi-wall shields like the classic Whipple shield [7]. A representative frame sequence from one of these cameras is shown in Figure 1. This sequence of images is from the demise of a CFRP projectile with the dimensions of 0.671 mm length × 2.402 mm diameter and an impact speed of 6.99 km/s. In the first frame of Figure 1, the intact projectile's image is clearly caught prior to impact, and along with the other orthogonal camera images (not shown), these cameras allow precise determination of the cylindrical axis orientation. For this shot, the projectile's central axis is pitched 10.3° from the velocity vector.
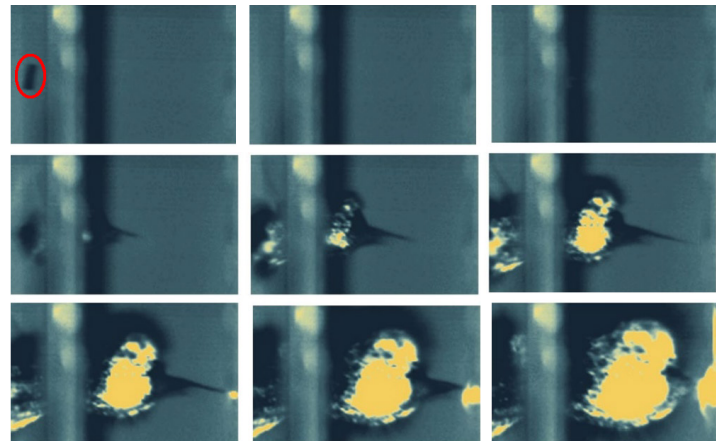

Figure 1. A representative array of frame captures from a CFRP projectile with L:D of 3.58:1. The interframe spacing is 0.4 microseconds. The projectile prior to impact is circled in red.

In the Table, a total of 83 shots using this experimental set up have been performed to provide damage and penetration data for various shield categories commonly used in orbital flight. Each of the targets are placed in the target mounting fixture and imaged throughout the impact. Figure 2 shows images of representative non-spherical projectiles used in these tests. These projectile types include: CFRP, stainless steel, and copper, as well as new projectile materials that are being added such as aluminum projectiles.
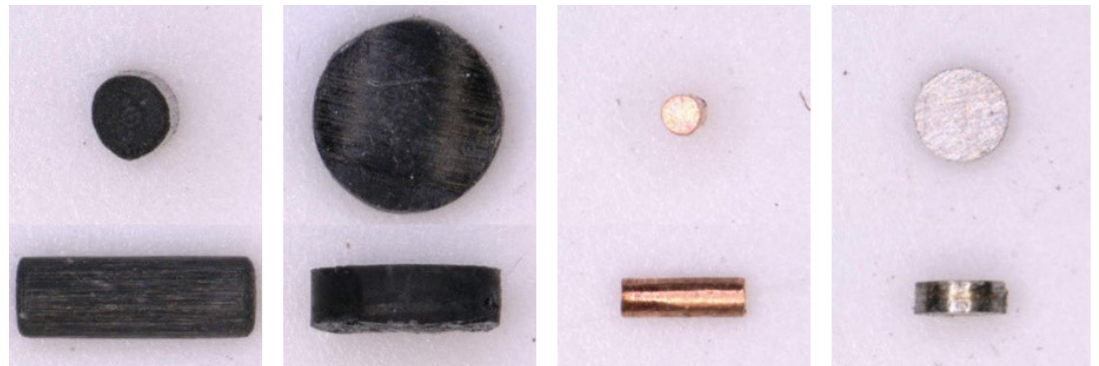

Figure 2. Representative images of RCC projectiles (L-R): CFRP with L:D~3:1; CFRP with L:D~1:3; copper with L:D~3:1; and stainless steel with L:D~1:3

The categories of shield types shown in the Table have focused on generalizable shield types that will form the foundation of generalized equations not specific to any vehicle (ODQN, vol. 25, issue 4, pp. 2-5). Representative images of the four generalized shields of the Table are shown in Figure 3. The first generalized shield type is the general double-wall shield, shown first from the left. The double-wall shield type is the most extensively used shield type that NASA currently assesses for spacecraft reliability and survivability assessments. The second generalized shield type is

Figure 3. Representative images of the four generalized classes of shields considered thus far (L-R): double-wall (Whipple) shield; monolithic metallic shield (copper plate); monolithic porous shield (AETB); and multi-wall shield (stuffed-Whipple).

monolithic, metallic materials with a representative copper plate. This shield type is representative of exposed structural elements like tanks and docking tunnels, and in the case of monolithic copper, represents exposed conductors. The third generalized shield type is porous, monolithic materials. This shield type is

7

Whipple Shields

representative of thermal materials that protect vehicles from the intense thermal environment of atmospheric reentry. In the third image, the representative for this class of shield is the alumina-enhanced-thermal-barrier (AETB). The final shield category is the multi-wall shield structure (*i.e.*, stuffed-Whipple shield) as shown farthest to the right. The stuffed-Whipple is the standard metallic, double-wall (Whipple) shield with intermediate fabric layers of Nextel™ and Kevlar® included to increase ballistic performance of the shield [5].

Each shield category has been selected based upon its impact physics. The double-wall shield system has been widely studied for impacts using spherical projectiles [5]. This configuration allows spreading of the debris cloud between the first wall (bumper) and rear (shield) walls; a much lighter wall is necessary to shield against a given projectile than for a single-wall shield, resulting in an overall lower-mass shield system. In general, the spherical shape of the projectile assists the spread of material through two mechanisms. First, the spherical shape is the most concentrated mass (meaning more of the projectile will see a strong shock wave, leading to more melt and/or vaporization); second, the spherical shape helps laterally spread debris because of divergent shock waves in the bumper and reflecting shock waves from the curved rear surface of the projectile [8]. The next two categories: monolithic-metallic and monolithic-porous, do not have an expansion gap, resulting in only a measurement of cratering in the material, though monolithic-porous results in a much deeper cratering process. The final multi-wall structure does have an expansion gap, but each subsequent layer of the shield faces less material with non-spherical characteristics.

Even with these simplifications, the parameter space facing the implementation of non-spherical projectiles is vast. As a result of these high complexities, an approach for non-spherical projectiles uses a symbiotic approach combining experimental data and numerical simulation results to extend the experimental conditions to a large variety of impact conditions (projectile orientation, impact speed, impact angle/obliquity, and projectile density). In this context, the experiments performed to-date with non-spherical projectiles are used to verify numerical simulation models, which give informed extrapolations to other impact conditions for BLE development. Future HVI testing efforts will continue to employ these techniques to develop anchor points for model development of shield response against non-spherical projectile impacts.

References

1. Polk, M., *et. al.* "Orbital debris assessment testing in the AEDC Range G," Procedia Engineering, 103, pp. 490-498 (2015).

2. Liou, J.-C., *et. al.* "DebriSat-A planned laboratory-based satellite impact experiment for breakup fragment characterization," International Astronautic Congress Proceedings, IAC-16. A6.2.8x35593 (2016).

3. Fitz-Coy, N., *et. al.* "Characterization of debris from the DebriSat hypervelocity test," 66th International Astronautical Congress at Jerusalem, Israel, IAC-15-A6.2.9x30343, pp. 1-10 (2015).

4. Cowardin, H.M., et. al. "Optical characterization of DebriSat fragments in support of orbital debris environment models," J Astronaut Sci 68, 1186–1205 (2021).

5. Christiansen, E.L. "Meteoroid/debris shielding," NASA/TP-2003-210788 (2003).

6. Christiansen, E.L., *et. al.* "The NASA JSC Hypervelocity Impact Technology (HVIT) Office," 2nd International Orbital Debris Conference Papers 2023, 6087, (2023).

7. Whipple, F.L. "Meteorites and space travel," Astronomical Journal, 52:1161, 131 (1947).

8. Miller, J.E., *et al*. "Analytic ballistic performance model of Whipple shields," Procedia Engineering, 103, pp. 389-397 (2015). ♦

Nextel™ is a trademark of 3M Company. Kevlar® is a registered trademark of E. I. du Pont de Nemours and Company or its affiliates. Trade names and trademarks are used in this report for identification only. Their usage does not constitute an official endorsement, either expressed or implied, by the National Aeronautics and Space Administration.

MEETING REPORT

Spacecraft Anomalies and Failures 2024 Workshop, 27-28 March 2024

The Spacecraft Anomalies and Failures (SCAF) 2024 Workshop was held 27-28 March 2024. The SCAF Workshop is an annual event organized by NASA's Space Environments Technical Discipline Team in collaboration with the National Reconnaissance Office (NRO). The goal of the workshop is to bring together civil, military, industry, and academia personnel for an opportunity to connect around common interests in space system anomalies and failures. NASA hosted the public session at Goddard Space Flight Center (GSFC), and speakers presented examples of space environments and their relationship to spacecraft anomalies; case studies of anomaly and failure investigations for NASA and NOAA spacecraft; description of processes used to mitigate anomalies for NASA programs; and examples of analytical techniques applied to radiation events archived in GSFC's Spacecraft Orbital Anomaly Report System. There were 385 participants registered for Day 1, demonstrating a continued community interest and support for the workshop. More information can be found at https://www.nasa.gov/nase/conferences/scaf2024/. ♦

UPCOMING MEETINGS

13-21 July 2024: Committee on Space Research (COSPAR) 2024, BEXCO, Busan, Korea

The 45th Scientific Assembly of the Committee on Space Research (COSPAR) Scientific Assembly will convene in the Busan Exhibition and Convention Center, BEXCO. The COSPAR panel on Potentially Environmentally Detrimental Activities in Space (PEDAS) will conduct a program entitled "A Sustainable Space Exploration: from the Mitigation of Space Debris in Earth's Orbit to the Safeguard of Planetary Environments." The main topics to be discussed in the PEDAS.1 sessions will include orbital debris observations and measurements; environmental models and databases; modeling and risk analysis; mitigation and remediation; sustainable space activities; national and international standards and guidelines; mega-constellation impact on astronomy; pollution of the Earth's atmosphere by rocket launches and reentries; cis-lunar space; and the Lunar and Martian environments. The abstract submission period closed on 09 February 2024. Please see the PEDAS.1 session website at https://www.cospar-assembly.org/admin/session_cospar.php?session=1295 and the Assembly website at: https://www.cospar2024.org/.

8-13 September 2024: 17th Hypervelocity Impact Symposium (HVIS), Tsukuba, Japan

The Hypervelocity Impact Symposium (HVIS) is a biennial event organized by the Hypervelocity Impact Society that serves as the principal forum for the discussion, interchange, and presentation of the physics of high- and hypervelocity impact and related technical areas. Orbital debris-related presentations include fracture and fragmentation; launchers and diagnostics; penetration mechanics and target response; hypervelocity phenomenology studies; material response; meteoroid and debris shielding and failure analysis; and theoretical applied mechanics relevant to hypervelocity impact. This year's symposium will feature a special session on hypervelocity phenomena related to planetary protection. The abstract submission deadline passed on 01 February 2024. Additional information for the 17th Symposium is available at https://hvis2024japan.jp/.

17-20 September 2024: 25th Advanced Maui Optical and Space Surveillance Technologies Conference (AMOS), Maui, Hawaii, USA
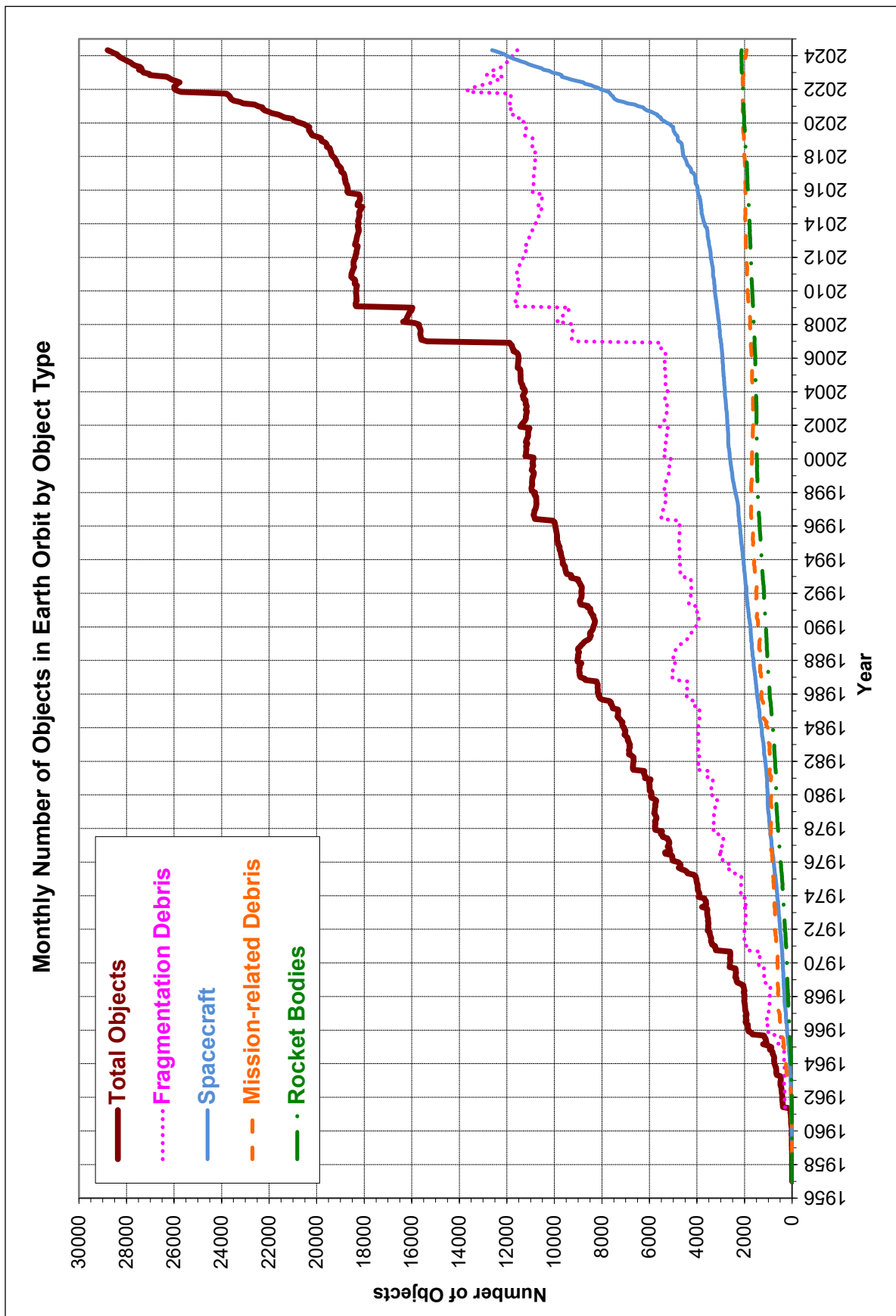
The technical program of the 25th Advanced Maui Optical and Space Surveillance Technologies Conference (AMOS) will focus on subjects that are mission critical to space situational awareness. The technical sessions include papers and posters on space debris; space situational/space domain awareness (SDA); SDA systems and instrumentation; astrodynamics; satellite characterization; space weather; and related topics. The abstract submission deadline was 01 March 2024. Registration for this hybrid conference opened in April 2024 for in-person and virtual attendees. Additional information about the conference is available at https://amostech.com.

## 14-18 October 2024: 74th International Astronautical Congress (IAC), Milan, Italy

The 75th IAC will convene in 2024 with a theme of "Responsible Space for Sustainability." The IAC's 22nd IAA Symposium on Space Debris will cover space debris detection, tracking and characterization; modeling; risk analysis; hypervelocity impact and risk assessments; mitigation; post-mission disposal and space debris removal; operations in the space debris environment; political, legal, institutional, and economics aspects of mitigation and removal; and orbit determination and propagation. Interactive presentations on space debris topics will also be provided to allow more digital display capabilities for attendees. The abstract submission deadline was 28 February 2024. Additional information for the 2024 IAC is available at https://www.iafastro.org/events/iac/international-astronautical-congress-2024/ and https://www.iac2024.org/. ♦

Announcements

The ODPO has an opening for a postdoctoral fellow via the NASA Postdoctoral Progam. This position would support an *in situ* sensor in development to characterize the small (millimeter-sized) orbital debris environment in low Earth orbit. Opportunities are available to support the development of the sensor and provide oversight and analyses that directly support future flight missions. For more information on this position, please see the request.

Monthly Number of Objects in Earth Orbit by Object Type

Legend:
- **Total Objects**
- **Fragmentation Debris**
- **Spacecraft**
- **Mission-related Debris**
- **Rocket Bodies**

X-axis: **Year** (1956–2024)
Y-axis: **Number of Objects** (0–30000)

Monthly Number of Cataloged Objects in Earth Orbit by Object Type as of 9 June 2024. This chart displays a summary of all objects in Earth orbit officially cataloged by the U.S. Space Surveillance Network. "Fragmentation debris" includes satellite breakup debris and anomalous event debris, while "mission-related debris" includes all objects dispensed, separated, or released as part of the planned mission

Monthly Mass of Objects in Earth Orbit by Object Type

Legend:
- Total Objects
- Spacecraft
- Rocket Bodies
- Fragmentation Debris
- Mission-related Debris
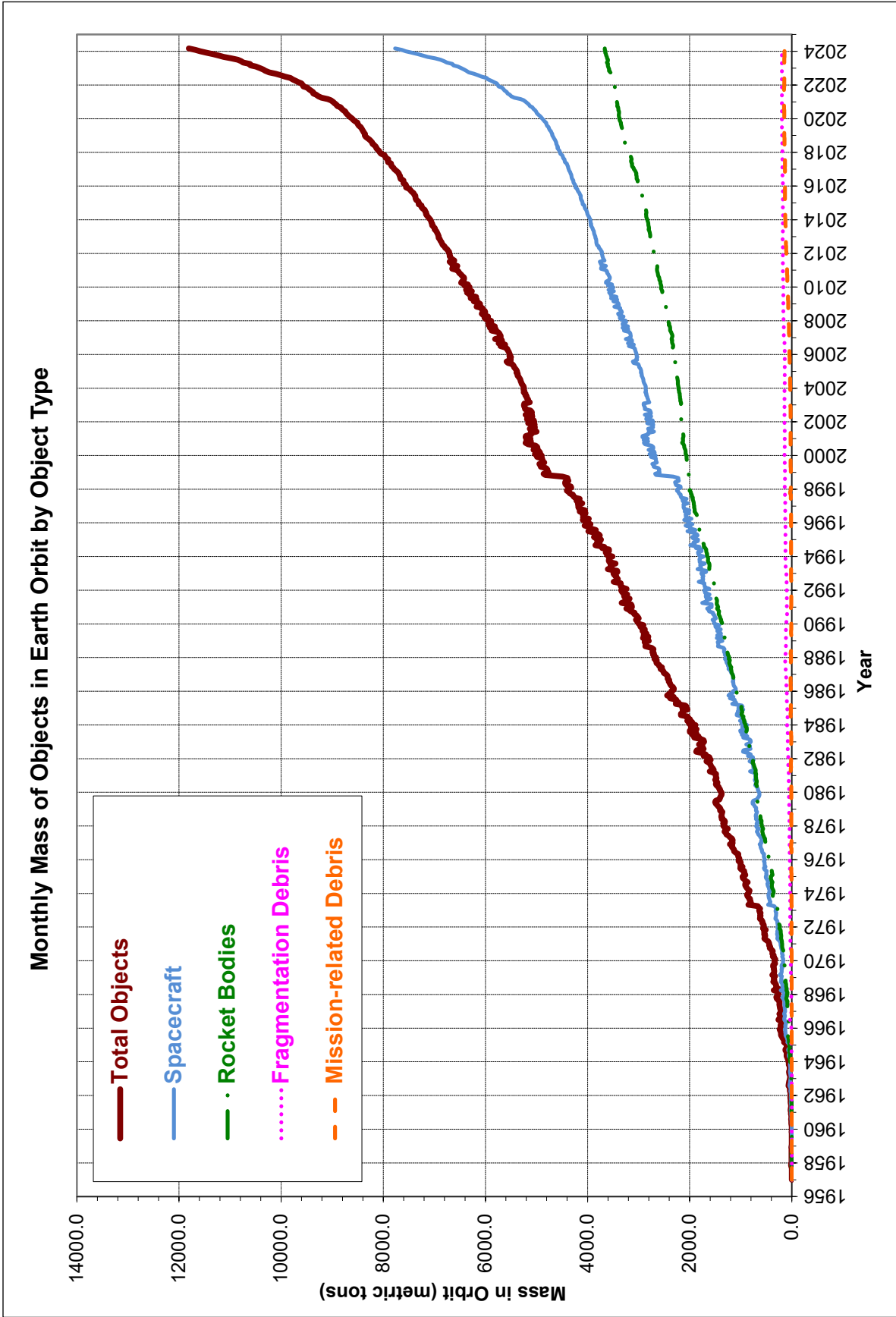
Monthly Mass of Objects in Earth Orbit by Object Type as of 9 June 2024. This chart displays the mass of all objects in Earth orbit officially cataloged by the U.S. Space Surveillance Network.

SATELLITE BOX SCORE
(as of 4 June 2024, cataloged by the U.S. SPACE SURVEILLANCE NETWORK)

Country/ Organization	Spacecraft*	Spent Rocket Bodies & Other Cataloged Debris	Total
CHINA	677	4288	4965
CIS	1568	5452	7020
ESA	97	28	125
FRANCE	90	532	622
INDIA	110	97	207
JAPAN	209	107	316
UK	697	1	698
USA	8114	4980	13094
OTHER	1183	81	1264
Total	**12745**	**15566**	**28311**

* active and defunct

Visit the NASA
Orbital Debris Program Office Website
www.orbitaldebris.jsc.nasa.gov

Intl. = International; SC = Spacecraft; Alt. = Altitude; Incli. = Inclination; Addnl. = Additional; R/B = Rocket Bodies; Cat. = Cataloged
Notes: 1. Orbital elements are as of data cut-off date 30 April. 2. Additional spacecraft on a single launch may have different orbital elements. 3. Additional uncataloged objects may be associated with a single launch.

INTERNATIONAL SPACE MISSIONS
1 February 2024 – 30 April 2024

Intl.* Designator	Spacecraft	Country/ Organization	Perigee Alt. (KM)	Apogee Alt.(KM)	Incli. (DEG)	Addnl. SC	Earth Orbital R/B	Other Cat. Debris
1998-067	ISS dispensed objects	Various	412	416	51.6	10	0	0
2024-023A	OBJECT A	PRC	595	608	50.0	10	1	0
2024-024A	OBJECT A	TBD	497	507	97.4	8	0	2
2024-025A	PACE	US	674	677	98.1	0	0	0
2024-026A	COSMOS 2575	CIS	328	340	96.7	0	1	0
2024-027A	STARLINK-31317	US	481	483	53.2	21	0	0
2024-028A	HBTSS-SV2	US	992	1005	40.0	5	0	0
2024-029A	PROGRESS MS-26	CIS	412	416	51.6	0	1	0
2024-030A	IM-1 (ODYSSEUS)	US	LUNAR LANDING			0	0	0
2024-031A	STARLINK-31373	US	481	483	53.2	21	0	0
2024-032A	CE-SAT-IE	JPN	669	674	98.1			
2024-032B	VEP-4	JPN	670	672	98.1			
2024-032C	TIRSAT	JPN	662	672	98.1			
2024-033A	INSAT 3DS	IND	35738	35835	0.1	0	1	0
2024-034A	ADRAS-J	JPN	556	618	98.2	0	2	0
2024-035A	TELKOMSAT 113BT	INDO	35781	35793	0.0	0	1	0
2024-036A	STARLINK-31468	US	481	481	53.2	21	0	0
2024-037A	TJS-11	PRC	35769	35803	5.4	0	1	0
2024-038A	STARLINK-30996	US	487	489	43.0	23	0	0
2024-039A	METEOR M2-4	CIS	814	822	98.6	17	1	1
2024-040A	HG-01	PRC	35772	35800	0.0	0	1	0
2024-041A	STARLINK-31265	US	487	489	43.0	22	0	0
2024-042A	DRAGON ENDEAVOUR 5	US	412	416	51.6	0	0	0
2024-043A	HORACIO	SPN	585	604	97.8	50	0	0
2024-044A	STARLINK-31312	US	443	445	43.0	22	0	0
2024-045A	STARLINK-31439	US	442	446	43.0	22	0	0
2024-046A	STARLINK-31603	US	446	448	53.2	22	0	0
2024-047A	STRIX-3	NZ	551	577	97.6	0	2	0
2024-048A	OBJECT A	PRC	971	225193	27.6	0	1	1
2024-049A	STARLINK-31304	US	443	445	43.0	22	0	0
2024-050A	STARLINK-31659	US	447	448	53.2	19	0	0
2024-050W	USA 350	US	312	315	53.2			
2024-050X	USA 351	US	312	315	53.2			
2024-051A	QUEQIAO-2	PRC	LUNAR ORBIT			0	1	0
2024-051C	TIANDU-1	PRC	LUNAR ORBIT					
2024-051D	TIANDU-2	PRC	LUNAR ORBIT					
2024-052A	OBJECT A	PRC	1131	1140	50.1	5	1	0
2024-053A	USA 352	US	NO ELEMS. AVAILABLE			0	2	0
2024-053B	MOLA	US	508	515	50.0			
2024-053C	AEROCUBE 16A	US	508	514	50.0			
2024-053D	AEROCUBE 16B	US	508	514	50.0			
2024-054A	DRAGON CRS-30	US	412	416	51.6	0	0	0
2024-055A	SOYUZ MS-25	CIS	412	416	51.6	0	1	0
2024-056A	STARLINK-31463	US	443	445	43.0	22	0	0
2024-057A	STARLINK-31402	US	443	445	43.0	22	0	0
2024-058A	YUNHAI 3-02	PRC	847	849	98.8	0	1	0
2024-059A	EUTE 36X	EUTE	2302	63931	19.5	0	1	0
2024-060A	STARLINK-31605	US	443	445	43.0	22	0	0
2024-061A	RESURS P4	CIS	468	470	97.2	0	1	0
2024-062A	STARLINK-31641	US	437	439	53.2	21	0	0
2024-063A	OBJECT A	PRC	493	501	35.0	0	1	0
2024-064A	STARLINK-31534	US	443	445	43.0	22	0	0
2024-065A	STARLINK-11087	US	354	355	53.2	20	0	0
2024-066A	TSAT-1A	IND	588	597	45.6	10	0	0
2024-067A	USA 353	US	NO ELEMS. AVAILABLE			0	1	0
2024-068A	STARLINK-31617	US	414	421	43.0	22	0	0
2024-069A	DUMMY SAT 3/ ORION	CIS	36052	36466	0.1	2	0	1
2024-070A	WSF-M	US	820	828	98.7	0	0	0
2024-071A	STARLINK-31753	US	421	423	43.0	22	0	0
2024-072A	OBJECT A	PRC	498	498	97.5	0	0	0
2024-073A	STARLINK-31635	US	370	372	43.0	22	0	0
2024-074A	STARLINK-31734	US	347	350	43.0	22	0	0
2024-075A	OBJECT A	PRC	491	502	35.0	0	1	0
2024-076A	STARLINK-31747	US	330	332	43.0	22	0	0
2024-077A	NEONSAT-1	SKOR	507	528	97.4	0	2	0
2024-077B	ACS 3	US	993	1022	97.4			
2024-078A	SZ-18	PRC	376	381	41.5	0	1	3
2024-079A	OBJECT A	TBD	22925	22984	54.7	0	1	0
2024-079C	OBJECT C	TBD	22915	22947	54.7			
2024-080A	STARLINK-31770	US	315	317	43.0	22	0	0

12